Climatic Change
https://doi.org/10.1007/s10584-018-2225-z

Diversity in global patterns of observed precipitation variability and change on river basin scales

A conditional quantile approach

Anne M. Lausier[1] · **Shaleen Jain**[1]

Received: 28 September 2017 / Accepted: 13 May 2018

Abstract Comprehensive characterization of diversity in global patterns of precipitation variability and change is an important starting point for climate adaptation and resilience assessments. Capturing the nature of precipitation probability distribution functions (PDF) is critical for assessing variability and change. Conventional linear regression-based analyses assume that slope coefficients for the wet and dry tails of the PDF are consonant with the conditional mean trend. This assumption is not always borne out in the analyses of historical records. Given the relationship between sea surface temperature (SST) and precipitation, recent trends in global SST complicate interpretations of precipitation variability and risk. In this study, changes in the PDF of annual precipitation (1951–2011) at the global river basin scale were analyzed using quantile regression (QR). QR is a flexible approach allowing for the assessment of precipitation variability conditioned on the leading empirical orthogonal function (EOF) patterns of global SST that reflect El Niño–Southern Oscillation and Atlantic Multi-decadal Oscillation. To this end, the framework presented (a) offers a characterization of the entire PDF and its sensitivity to the leading modes of SST variability, (b) captures a range of responses in the PDF including asymmetries, (c) highlights regions likely to experience higher risks of precipitation excesses and deficits and inter-annual variability, and (d) offers an approach for quantifying risk across specified quantiles. Results show asymmetric responses in the PDF in all regions of the world, either in single or both

Electronic supplementary material The online version of this article (https://doi.org/10.1007/s10584-018-2225-z) contains supplementary material, which is available to authorized users.

Supported by US NSF grants: DGE 1144205 & CAREER 1055934

✉ Anne M. Lausier
anne.lausier@maine.edu

Shaleen Jain
shaleen.jain@maine.edu

[1] Department of Civil and Environmental Engineering, University of Maine, Orono, ME, USA

Published online: 04 June 2018

tails. In one instance, QR detects a differential response to the leading patterns of SST in the Tana basin in eastern Africa, highlighting changes in variability as well as risk.

1 Introduction

Precipitation is a primary component of the freshwater budget across various spatial and temporal scales. Numerous human and environmental systems, such as agriculture, industry, and recreation are sensitively linked to precipitation variability. Furthermore, freshwater-reliant ecosystems provide a range of services, such as resource provision, nutrient cycling, water purification, flood protection, and have cultural importance (Brauman et al. 2007; Chang and Bonnette 2016). In the multifarious contexts noted above, estimation of likelihood of precipitation excesses and deficits over decision-specific thresholds is of interest. This includes characterization of precipitation functional-forms from which PDF parameters are modeled, including changes in central tendency, and position of upper and lower tails, which are critical to assessing variability.

Changing patterns of precipitation and its extremes at regional (Bradley et al. 1987; Groisman and Easterling 1994) and global (Jones 1988; Diaz et al. 1989; Karl et al. 1995) scales have been documented, with changes in precipitation trends linked with sea surface temperature (SST) variability studied extensively. El Niño–Southern Oscillation (ENSO) is most influential in determining global precipitation variability (Gershunov and Barnett 1998; Dai and Wigley 2000; Kenyon and Hegerl 2010; Sun et al. 2015). However, there are additional patterns of ocean-atmospheric variability with regional effects, such as the North Atlantic Oscillation (NAO), Pacific Decadal Oscillation (PDO), and the Atlantic Multi-decadal Oscillation (AMO) (Scaife et al. 2008; Nigam et al. 2011; Whan and Zwiers 2017), which are associated with global-scale precipitation changes with regional effects over the USA, Africa, India, and Europe (Enfield et al. 2001; Sutton and Hodson 2005; Knight et al. 2006).

Given the sensitivities of the precipitation PDF to SSTs, the nature of SST oscillations and combined influence of patterns complicates assessments of precipitation variability. The SST patterns often exhibit slow variations and persist on seasonal to annual time scales. For example, ENSO oscillates between cold and warm phases on a 3–7-year time scale (Deser et al. 2010), while AMO is characterized by slow variations over a 65–80-year period (Enfield et al. 2001). The effect of SSTs on the functional form of precipitation can be to minimize or amplify sensitivities, with persistence of pattern phases implying that locations with significant sensitivities to SST patterns may experience impacts with increased frequency.

Despite these recorded relationships, widely used linear statistical techniques, such as linear regression (LR), rely on measures of central tendency and constant variance, assuming that changes in the mean characterize location changes over the entire distribution. Precipitation distributions often violate these assumptions, and changes in the mean often do not characterize changes in extremes (Kim and Jain 2011; Lee et al. 2013). An example of such an application is Observations: Surface and Atmospheric Climate Change (Trenberth et al. 2007) in the Intergovernmental Panel on Climate Change (IPCC) Climate Change 2007 Working Group I Report. Figure 3.13 on pg. 256 of the report (https://www.ipcc.ch/publications_and_data/ar4/wg1/en/ch3s3-3-2-2.html) assesses mean annual precipitation trends, implying that the risk of a high or low annual total is proportionally increasing or decreasing with the mean and that the variance is time-invariant. Furthermore, with

precipitation having a significant relationship with other drivers, such as SST, specifying year as the only covariate may not adequately characterize the distributional changes in annual total precipitation, underscoring the need for more flexible approaches.

This study reappraises the nature and type of changes in the magnitude of annual precipitation on the river basin scale. Climate risks are characterized as the changes in likelihood of precipitation excesses and deficits, requiring particular assessment of shifts in the extrema of the precipitation PDF. Unless otherwise noted, in this study, risk signifies changes in likelihood. The PDF aids computation of exceedance and non-exceedance probabilities for a given precipitation threshold. The selection of thresholds may depend upon either (a) a specification of precipitation magnitude when exceeded constitutes an extreme event (e.g., an annual precipitation total exceeding two standard deviations above the mean) or (b) for a specified exceedance probability (e.g., 1% or 100-year return period): the extreme annual precipitation value consistent with the exceedance probability. For the remainder of this study, extreme wet and dry conditions are defined as large excursions from long-term median estimates based on historical data. Consequently, tail probabilities represent the likelihood of such events. Shifts (changes in location) in the tails of the distribution indicate a higher or lower probability of an extreme annual total. A quantile regression (QR) model (Koenker and Bassett 1978; Koenker 2017) was applied as an alternative to LR approaches as it (a) is robust to outliers, (b) does not make distributional assumptions, (c) characterizes a variety of shifts across the entire distribution (including extremes), (d) can be used to quantify changes for any specified thresholds (quantile) of interest for coupled human-environmental contexts, and (e) offers insight into exposure and consequence via derivation of spatial patterns of global precipitation sensitivity and changing likelihood induced by SST conditions. In this work, global patterns of conditional quantile response were estimated, with attention to changes in risk. Salient questions addressed in this study are as follows:

1. Based on a quantile regression approach, what are the linkages between river basin scale precipitation and coherent patterns of global sea surface temperature variability?
2. At regional and global scales, what are the detailed spatial characteristics of precipitation variability for lower, median, and upper quantile levels?
3. In what ways can a quantile regression approach be used to estimate the influence of climate variability patterns on conditional risk likelihoods for precipitation?

The rest of this paper is organized as follows. Firstly, linkages between precipitation and climate variability are delineated (Section 2.1) followed by an examination of the advantages of a quantile regression approach over ordinary least squares regression for characterizing distributional asymmetries (Sections 2.2–2.4). Next, an assessment of the linkages between annual precipitation and the coherent patterns of climate variability at the basin scale globally and regionally is presented (Sections 3.1–3.2). Lastly, the use of SST variability patterns for estimating conditional risk likelihoods is explored (Section 3.3).

2 Data and methods

2.1 Data and study region

Annual precipitation for 405 river basins around the world were analyzed (Fig. S1) for the 1951–2011 time period on a June–May annual year. A June–May annual designation

captures the expression of El Niño and La Niña events as well as preserves the primary wet season for most basins (Fig. S2). The river basin delineations used for precipitation analysis are from the 405 Major Water Basins of the World dataset obtained from the Global Runoff Data Centre (Global Runoff Data Centre (GRDC) 2007). Global gridded monthly total precipitation dataset at a 0.5° x 0.5° resolution (CRU TS3.22) were obtained from the UK Natural Environment Resource Council's British Atmospheric Data Centre (NERC-BADC), and were produced by the University of East Anglia Climatic Research Unit (Harris et al. 2014). SST data monthly grids were obtained from National Oceanic and Atmospheric Administration (NOAA) Extended Reconstructed Sea Surface Temperature V3b dataset with 2.0° x 2.0° resolution (Smith et al. 2008).

Monthly precipitation data were aggregated to produce annual totals, and were areally averaged over the global river basins. Monthly SST data were aggregated at each grid point to produce an annually resolved dataset, and the long-term trend was removed. To derive the leading SST patterns, empirical orthogonal functions (EOFs) were produced from the detrended data. A correlation matrix was used over a covariance matrix as large variance differences between elements can lead to a few elements dominating the first few patterns (Jolliffe 2002). To assess the relationship between the leadings patterns of SST and precipitation variability, precipitation EOFs were produced in a similar manner. Additional details can be found in Online Resource 1.

2.2 Annual precipitation variability and change: conditional quantile functions

QR is a robust approach to characterizing changes across the range of precipitation thresholds, including the upper and lower tails. Unlike LR, QR detects responses in upper and lower quantiles that may differ in magnitude and/or direction to the mean, with different implications for variability and risk. Additional details of the methodology and advantages over LR are offered in Koenker (2005). The linear QR model has the form

$$y_i = \beta_0^{(\tau)} + \beta_1^{(\tau)} x_i + \epsilon_1^{(\tau)}, \tag{1}$$

where $\beta_0^{(\tau)}$ is the intercept and $\beta_1^{(\tau)}$ is the slope coefficient for the selected quantile τ, which ranges from 0 to 1. The reader should note that τ is not read as an exponent. In this approach, QR allows conditional estimates of precipitation levels (at quantile τ) that are larger than τ and smaller than $(1 - \tau)$ proportion of historical data. In this study, a no-cross restriction was placed on quantile coefficient values for each covariate, as the crossing of quantile regression lines provides erroneous results (Bondell et al. 2010). To assess significance, a permutation test was conducted, where y_i was sampled with replacement and β_i was calculated ($n = 1000$) producing a distribution of coefficient values. A percentile test (0.95, 0.05) was used to determine the significance of β_i. In an effort to characterize the relative sensitivity of basin scale precipitation to leading patterns of SST variability, the QR approach was used due to its ability to clarify the quantile-by-quantile conditional relationship. To this end, prior to introducing SST covariates (Sections 3.1–3.2), several illustrative cases are presented to aid a clearer interpretation of QR coefficients (both their magnitude and signs) across select quantiles.

2.3 Distributional characterization of synthetic data

To demonstrate the diversity of responses captured in the QR approach, synthetic precipitation data were generated to mimic geophysical records of the same length as the historical data. The synthetic data exhibit the combinations of upper ($\tau = 0.8$) and lower ($\tau = 0.2$)

tail trends; some or all of these may be found in historical records. QR was conducted on the datasets across the quantiles, $\tau = 0.2$, 0.5 (median), and 0.8, conditioned on time only, and compared to LR results. Figure 1a, e, i represents the changes implied by LR, where the entire PDF symmetrically shifts location to a higher or lower magnitude, or undergoes no significant change. However, in both *a* and *i*, changes in $\tau = 0.2$ and 0.8 are asymmetric, indicating differences in distributional probabilities in contrast to LR. *d* is an example where there is only an increase in the position of $\tau = 0.8$. This implies both increased variability, and probability of wet extremes. *b, f,* and *h* also exhibit single-tailed changes with *b* and *f* showing decreases in variability, while *h* indicates an increased risk of a dry year and increased variability. Similarly, *g* (*c*) indicates an increase (decrease) in variability due to diverging (converging) trends in the tails, where LR would find no significant change.

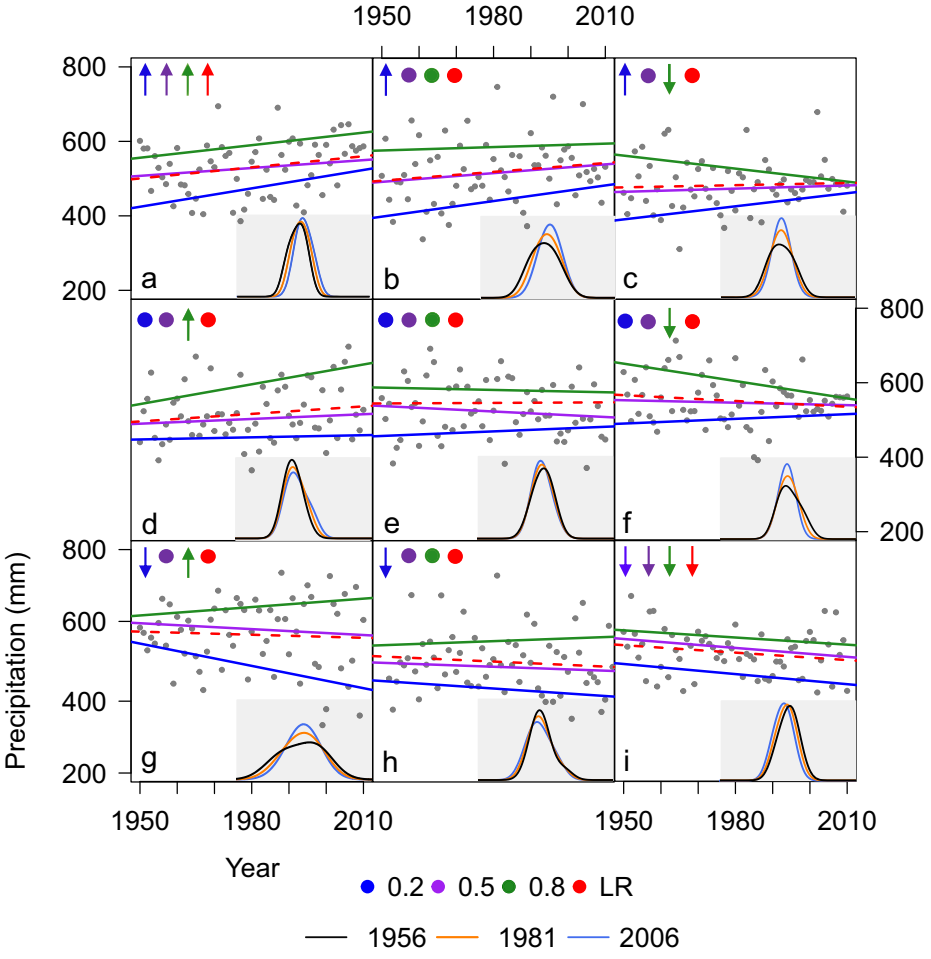

Fig. 1 Quantile regression of synthetic precipitation data (mm) conditioned on time ($\tau = 0.2$, 0.5, 0.8) to highlight the diversity of changes in environmental data. Linear regression estimations are shown using a dashed line. Arrows are color coded to represent the direction of changes for the respective conditional quantiles at a 90% significance level. Circles indicate no significant response. Shaded gray areas show empirical probability distributions for each case constructed for years 1956, 1981, 2006

Taken together, the diversity of changes discussed above underscore: (a) the fidelity with which the QR approach can be applied across cases of variability and change, (b) the ease with which one or more covariates (for example, time, ocean-atmospheric indices) can be incorporated, and (c) that QR can be readily tailored to be specific to the requisite quantiles or thresholds (including extremas—lower and upper tails) for place-based precipitation variability and change assessments. Additionally, over the range of quantiles, QR-derived regression coefficients constitute the basis to derive conditional probability distribution at a particular value of the climatic covariate (for example, El Niño conditions). Non-parametric estimation of conditional PDFs and their utility for risk analysis are discussed next.

2.4 Changing perspectives of conditional risk

In addition to characterizing the variety of possible quantile responses, conditional empirical probability distributions for each synthetic dataset were constructed for three different years to highlight differences in exceedance probabilities in the QR approach compared to LR (Fig. 1). Particularly when there is no significant change in the conditional mean, the results from the LR approach indicate no appreciable change across the entire range of quantiles. For environmental data, this can be restrictive and lead to mischaracterization of trends under LR approach. The QR approach allows for semi-independent shifts across quantiles implying changes in the risk of extremes in one or both tails of the probability distribution. For example, Fig. 1c shows an increase in $\tau = 0.2$ and decrease in $\tau = 0.8$ implying a decrease in variability over time. QR detects a decrease in $\tau = 0.8$ exceedance probability between 1956 and 2006, while a LR approach indicates an increase. A full example comparing the QR and LR exceedance probability differences over time for Fig. 1c can be found in Online Resource 1. While the reader should note that these PDFs are for illustrative purposes only, the QR approach shows that asymmetric changes in exceedance probability with increases (decreases) in upper threshold risk are not necessarily accompanied by proportional decreases (increases) in risk in corresponding lower thresholds.

2.5 Basin scale distributional changes

For a global analysis, the effects of SST variability on annual precipitation for the years 1951–2011 in the 405 global major river basins were assessed across the $\tau = 0.2, 0.5, 0.8$ quantiles using QR. Three covariates were used: year (1951–2011), and the SST time-series for the EOF analysis (EOF1, EOF2). All covariates are uncorrelated. The year covariate values were standardized and centered on 0, minimizing erroneous intercept calculations that may arise when using a wide range of values (Koenker 2005). Significance of each coefficient was determined at a $p \leq 0.1$ significance level (see Section 2.2 for details). A cautionary note to the reader is that trends in annual totals may not be indicative of the precipitation—SST relationship on monthly, seasonal, and episodic timescales.

3 Results

3.1 SST-precipitation relationships

SST has been shown to significantly correlate with precipitation globally (Diaz and Markgraf 2000). EOF results show that SST EOF1 and EOF2 explain 33.1 and 10.8% of the variance respectively (Table S1). SST EOF1 shows the highest anomalies in the Eastern

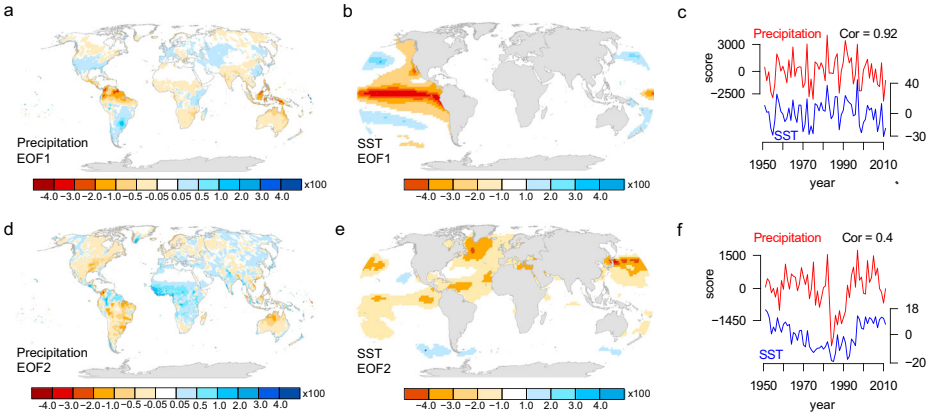

Fig. 2 **a** Leading empirical orthogonal function (EOF) of annual precipitation anomalies over land (June 1951–May 2011) based on the CRU_TS3.22 monthly precipitation grids. **b** Leading EOF of annual SST anomalies over the global oceans based on NOAA ERSST v3b monthly SST data set (June 1951– May 2011). **c** Comparison of global land precipitation EOF1 and SST EOF1 time-series. **d** Second precipitation EOF. **e** Second SST EOF. **f** Comparison of precipitation EOF2 and SST EOF2. Partial correlation with trend shows no change in correlation coefficients

Pacific (Fig. 2b) with SST EOF2 showing contrasting patterns in the north and mid-Atlantic and the northwestern Pacific to those in the mid-latitude Pacific (Fig. 2e). SST EOF1 has a correlation coefficient of $r = 0.93$ with the Niño-3.4 index, which is consistent with studies identifying EOF1 as capturing ENSO phenomenon (Deser et al. 2010; Messié and Chavez 2011), and $r = 0.72$ with the PDO index. EOF2 has a correlation coefficient of $r = 0.85$ with the AMO index and $r = -0.3$ with the PDO index. Precipitation EOF1 and EOF2 explain 15.4 and 5.3% of the variability (Table S1) with EOF1 showing highest correlations in North and South America, Indonesia, and Northern Australia (Fig. 2a) and EOF2 showing high correlations in sub-Saharan Africa, Northern Europe, and Australia (Fig. 2d). Comparison of the EOFs of SST and precipitation show high correlation between the first EOFs ($r = 0.92$) with the SST EOFs showing distinct covarying patterns with precipitation (Fig. 2c). SST EOF2 and precipitation EOF2 are moderately correlated ($r = 0.4$), but captures sensitivities in Africa, which have been linked to AMO (Fig. 2f). The SST EOF1 and EOF2 time-series were chosen for this study to be used as covariates in a QR analysis model as they explain the highest amount of SST variation, and have the highest correlation to physical modes and precipitation patterns. Additional details can be found in Online Resource 1.

3.2 Variability in quantile-specific SST–precipitation relationship

The relationship between SST variability and precipitation for the years 1951–2011 was assessed at $\tau = 0.2$, 0.5, and 0.8 quantiles in the 405 global major river basins by

$$\text{Annual precipitation}(\tau \mid x) = \beta_0^{(\tau)} + \beta_1^{(\tau)}\text{year} + \beta_2^{(\tau)}\text{EOF1} + \beta_3^{(\tau)}\text{EOF2} + \epsilon^{(\tau)}, \quad (2)$$

where $0 < \tau < 1$ represents the quantile, year is the time-series 1951–2011, and EOF1 and EOF2 are the respective SST time-series from the analysis of the global SST data.

The spatial patterns of precipitation response across quantiles (Fig. 3) identifies regions that are sensitive to EOF1 and EOF2, depicting the influence of phase and magnitude of SST

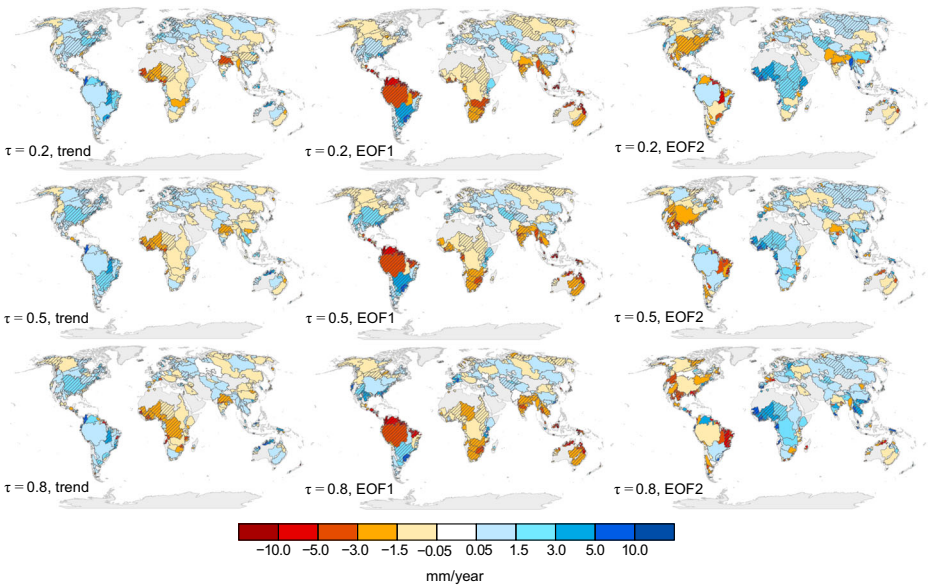

Fig. 3 Spatial distribution of basin-level precipitation quantile regression coefficients conditioned on years 1951–2011, EOF1, and EOF2 for select quantiles ($\tau = 0.2, 0.5, 0.8$) of basin areal average annual precipitation. Cross-hatch represents significance at $\alpha = 0.1$

on annual precipitation distributional response. The same analysis was conducted on annual precipitation data corrected for unequal areal extent of grids across latitudes, with negligible differences (Fig. S5). Coefficient signs and values across quantiles indicate that shifts are in the extremes of the distribution ($\tau = 0.2, 0.8$), and do not coincide with the slope of the estimated conditional mean function. EOF1 shows the most influence on precipitation with 62.0% of all basin area showing a significant response ($p \leq 0.1$) in at least one quantile, followed by EOF2 (44.1%), and trend (35.5%). Findings summarized by covariate include the following:

1. Precipitation shows significant increases across quantiles over time (trend) in the USA, South America, Africa, and decreases in southern Asia, and western Europe. In particular, both the Mississippi River basin in North America and the Parana Basin in South America show significant increases in all three quantiles evaluated.
2. EOF1 produces stronger magnitudes of response relative to the year covariate, with the PDF varying widely in shape and position from year to year. When EOF1 is in positive phase, corresponding to SST patterns in the tropical Pacific consistent with El Niño, there are strong negative responses in northern parts of South America, Africa, Southeast Asia, and Australia. Strong positive responses are seen in southern South America, and some moderate increases in the USA and Europe. For example, the Godavari and Ganges basins in the Indian subcontinent show negative responses consistent across quantiles.
3. When EOF2 is in positive phase, corresponding to warm temperatures in the Arctic and north Pacific, negative sensitivities are shown for $\tau = 0.5$ and 0.8 in the western USA, while negative responses in $\tau = 0.2$ are limited to the east. There are also strong to moderate positive responses in Africa, and in Southeast Asia in $\tau = 0.8$ only, while northern latitudes in Asia show only low magnitude positive response. For example, the

Yenisei basin shows a positive response of similar magnitude across quantiles, while the Guadalquivir basin in Spain shows a stronger positive response in $\tau = 0.8$ than $\tau = 0.2$ and 0.5 indicating an increase in variability.

With SST predictability, this spatial view highlights the overall sensitivity across quantiles, and the regional patterns of coherent precipitation variability. $\tau = 0.2$ and 0.8 coefficients that differ from each other in magnitude and sign from the median specifically demonstrate the value of the QR model with shifts evident across a range of locations. Wider distributions imply a higher uncertainty in anticipating the amount of precipitation, with implications for planning regarding water use in sectors, such as agriculture and industry. To this end, a continent-scale examination of upper and lower quantile SST-precipitation sensitivities with discussion of non-climatic factors, such as infrastructure, population, and water demand and sectoral uses that may amplify or temper risk can be found in Online Resource 2.

3.3 Combinations of upper and lower precipitation quantile responses

To explicitly categorize the diversity of quantile shifts, combinations of significant positive and negative, and non-significant changes in $\tau = 0.2$ and 0.8, hereafter referred to as typologies, were constructed for each covariate as demonstrated in the synthetic example (Section 2.3). These typologies (Fig. 4) offer a synthesized view of Fig. 3, allowing for a clearer spatial assessment of regions undergoing similar shifts in response to covariates. In the following, typologies will be referenced by Fig. 1 a–i. Typologies characterized by shifts in single quantiles (*b*, *d*, *f*, *h*) indicate higher variability (increase or decrease) than simultaneous shifts in the same direction. Conditional quantile responses are all for positive EOF1

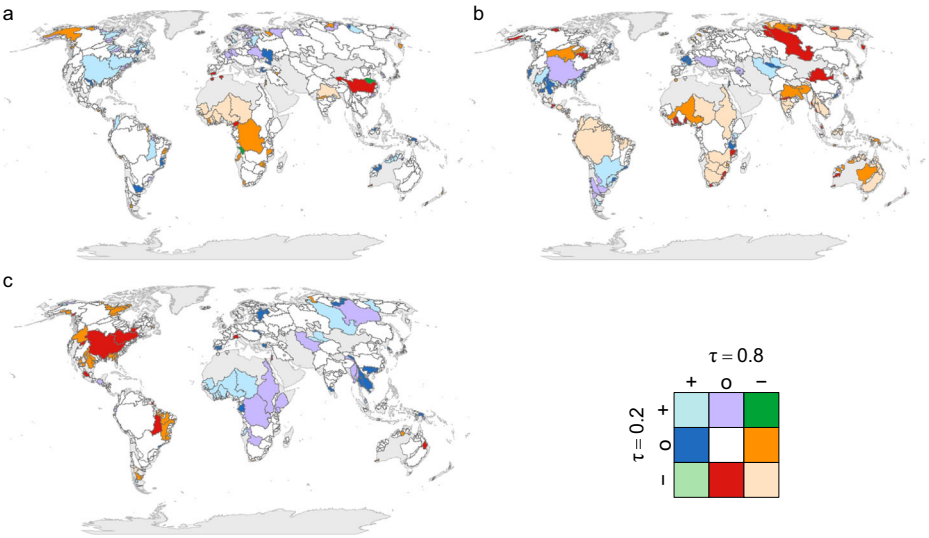

Fig. 4 Typologies of basin scale precipitation sensitivity to climate variability and change based on pairwise combinations of regression coefficients of $\tau = 0.2$ and 0.8. Basins are color coded according to combinations of positive (+), negative (-) significant response ($\alpha = 0.1$), and non-significant (o) response. Typologies are shown for annual precipitation totals (mm) for the 1951–2011 period conditioned on **a** years 1951–2011, **b** EOF1, and **c** EOF2

and EOF2 conditions. Responses in each quantile are opposite in sign for negative EOF1 and EOF2 conditions.

Globally, EOF1 and EOF2 show the most influence on precipitation and the year covariate the least with 56.7, 41.0, and 31.1% of basin land area showing a response respectively. The trend shows basins are largely characterized by either increases or decreases in both $\tau = 0.2$ and 0.8. (Fig. 4a). While trend captures temporal variability as well as other drivers in the system, the analysis in Section 3.1 demonstrated that distributional changes are more sensitive to EOF1 and EOF2, with larger covariate coefficients calculated.

3.3.1 Africa

Basins show either no response or a significant decrease in one or both quantiles over time, suggesting drier conditions. Precipitation changes conditioned on EOF1 generally show decreases except for eastern Africa. Conversely, EOF2 shows increases in quantile position. Key examples include the Pangani basin in Tanzania characterized by typology *a*, indicating increased probability of wet events. The Tana basin is characterized by type *a* under EOF1 and *b* under EOF2 indicating a decrease in probability of dry conditions. Western African basins, such as Niger, Lake Chad, and Sassandra, all show increases in both quantiles under EOF2. For EOF1, the Niger basin (*f*) shows a reduction in variability and probability of wet conditions. Lake Chad experiences a decrease in both quantiles. The continent generally experiences precipitation deficits (excesses) under positive EOF1 (EOF2).

3.3.2 Australia and Southeast Asia

Basins primarily show precipitation decreases under EOF1. For example, the Blackwood basin is characterized by *h* under EOF1 and *f* under EOF2. Type *h* indicates increased probability of dry conditions and higher variability, and *f* an decrease in wet conditions and lower variability. The Murray (*i*), Pahang (*h*), and Kinabatanga (*i*) basins similarly show decreases under for EOF1. Conversely for EOF2, there is no response in either the Kinabatanga or Murray basins and an increase in both quantiles (*a*) in the Pahang basin.

3.3.3 Asia

Most basins show precipitation decreases under EOF1 and increases under EOF2. For example, the Mekong shows decreases in both quantiles under EOF1 (*i*) and increase in $\tau = 0.8$ (*d*) under EOF2. Similarly, the Huang He (Yellow river) shows higher probability of dry conditions (*h*). The Ganges basin shows a decrease in $\tau = 0.8$ under EOF1 indicating a reduction in variability and wet conditions. Conversely, the Dongjiang basin shows an increase in $\tau = 0.8$ indicating an increase in variability and probability of wet conditions.

3.3.4 Western Europe

Few basins show significant response, with general increases under EOF1 and EOF2. For example, the Garonne basin in France shows increase in both quantiles (*a*) under EOF1, while the Rhone and Seine show increases in $\tau = 0.8$ only, indicating greater variability. The Thames shows a decrease in variability under EOF1 with an increase in $\tau = 0.2$ (*b*). The Guadalquivir basin is a key example of response to EOF2, showing an increase in $\tau = 0.8$ (*d*).

3.3.5 Eastern Europe and Russia

The basins with highest sensitivity are some of the least populated areas of the Northern Hemisphere. For example, the Yenisei basin shows a decrease in $\tau = 0.2$ under EOF1 (*h*) and an increase in both quantiles for EOF2 (*a*). This indicates a higher variability and probability of dry conditions for positive EOF1. Neighboring basins show similar results with decreases (increases) in either both or single-quantile positions for positive EOF1 (EOF2) conditions.

3.3.6 South America

EOF1 dominates the significant response with deficits in the north and excesses in the south. EOF2 has an influence along the east coast and southern tip, showing decreases in quantile position. For example, the Orinoco and Amazonas basins show decreases in both quantiles (*i*) indicating higher probability of deficits under EOF1. Conversely, the Parana and Uruguay basins show simultaneous increases (*a*). Under EOF2, the Parana basin shows a decrease in $\tau = 0.2$ (*h*).

3.3.7 North America

Precipitation changes over time show increases across the eastern USA and Canada, and decreases in northwestern Canada. EOF1 shows increases across the USA and central America and decreases in Canada, while EOF2 shows decreases. For example, the Sacramento and Colorado river basins show increases in both quantiles (*a*) and increase in $\tau = 0.8$ (*d*) respectively, showing increased probability of wet events and higher variability. Conversely, the Columbia river basin shows decreases in $\tau = 0.8$ (*f*) under EOF2. In the southeast USA, the Alabama & Tombigee and Suwannee basins show increases in both quantiles under EOF1 and decreases in $\tau = 0.8$ under EOF2. In the northeast USA, the Penobscot river basin shows a decrease in $\tau = 0.2$ (*h*) under EOF2 suggesting an increase in variability.

Typologies indicate the directionality of shifts, imply uncertainties, and highlight which drivers (EOF1 or EOF2) are most critical to these changes. For basins where EOF1 and EOF2 are both significant, distributional shifts are highly dependent on the commingling of covariate conditions. For example, the Tana basin in East Africa shows increases (*a*) when EOF1 is positive, and an asymmetric increase (*b*) when EOF2 is positive. When EOF1 and EOF2 are in the same phase, shifts are amplified depending on the magnitude, while opposite phase tempers the overall response and the directionality of shifts becomes dependent on covariate magnitudes. A related notion is the change in variability and risk implied by various combinations of EOF1, EOF2 conditions.

3.4 Assessment of distributional variability and conditional risk

The quantile-specific coefficients for EOF1 and EOF2 at a given location apportion the influence of each SST to risk. For given coefficients, the phase and magnitude of EOF1 and EOF2 determine the distribution of precipitation in a location, and thereby the risk likelihood at specified thresholds. To illustrate how EOF1 and EOF2 conditions jointly influence shifts in aspects of the precipitation distribution, quantile responses were calculated for the range of possible EOF combinations. This was applied to $\tau = 0.2, 0.5, 0.8$, and for the $\tau = 0.8 - 0.2$ quantile range illustrating shifts in location and distributional spread (variability). A case example for the Chad River basin in Northern Africa is presented (Fig. 5),

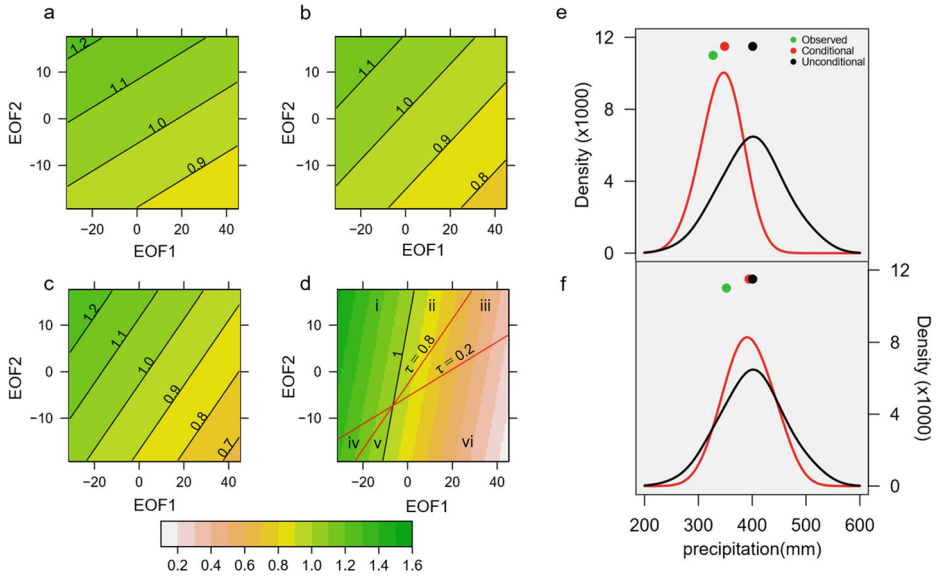

Fig. 5 Precipitation quantile position changes for possible EOF1, EOF2 values for the Chad River Basin, Africa. **a–c** ratio of conditional quantile regression coefficients of precipitation to unconditional quantiles. **a** $\tau = 0.2$, **b** $\tau = 0.5$, **c** $\tau = 0.8$. Ratios greater than 1 indicate an increase in exceedance probability compared to the unconditional quantile, and ratios less than one signify a decrease. **d** Classification of combination of changes in magnitude and direction of the upper and lower quantiles for EOF1, EOF2 pairs. Each red line marks the EOF1, EOF2 pairs for which the $\tau = 0.2, 0.8$ equals the unconditional $\tau = 0.2, 0.8$. Areas numbered (i–vi) show possible combinations of $\tau = 0.2, 0.8$ changes with implied changes for variability and risk (Table S3). A comparison of unconditional and conditional PDFs during distinct tropical Pacific sea surface temperature conditions: **e** strong El Niño event (1982–1983) and **f** median conditions (1990–1991). For significant departures in EOF1 and EOF2 median conditions, the precipitation distribution undergoes wide excursions from the unconditional state

with $\tau = 0.2, 0.5, 0.8$ significant to EOF1 and EOF2. The slopes of the contours indicate higher precipitation sensitivity to EOF2 in $\tau = 0.2$, and to EOF1 for $\tau = 0.8$ and the $\tau = 0.8 - 0.2$ quantile range. Distributional changes are characterized by six bounded areas depending on covariate phase and magnitude (Fig. 5d). For additional details, see Table S3. For any global SST condition, represented as a pair of EOF1 and EOF2 values, the appropriately conditioned precipitation conditional distribution can be determined for any basin.

For example, unconditional and conditional PDFs using EOF1 and EOF2 as covariates were constructed for 1982–1983 and 1990–1991. In the late 1970s, stronger ENSO amplitude was observed, with 1982–1983 being one of the most extreme El Niño events of the examined record. In a linear QR context with statistically significant regression slopes, significant departures from the median state of the covariate values can produce dramatic shifts in the conditional PDF. For the 1982–1983 event, EOF1 = 37.24 and EOF2 = − 5.06. This event falls in region vi of Fig. 5d, which for this basin is characterized by a decrease in variability, a decrease in risk of extreme wet conditions, and an increase in risk of extreme dry conditions (Table S3). The conditional distribution acknowledges that the probability of the precipitation total for 1982–1983 occurring is greater than in the unconditional distribution (Fig. 5e). Conversely, the 1990–1991 year is characterized by EOF1 and EOF2 conditions that do not depart significantly from the long-term median (EOF1= 4.15; EOF2= − 1.39).

Due to the small values, the quantile shifts are minimal (Fig. 5f). The observed value falls within the middle 60% of both distributions, with each representing a similar exceedance probability for the observed total. In the absence of EOF1 and EOF2 information, the unconditional distribution may over- or underestimate the likelihood of exceeding given thresholds for years with significant departures from mean conditions.

4 Summary and conclusions

The analysis presented considers the changes of the annual precipitation distribution conditioned on leading patterns of global SST variability for 405 major river basins. The results show that (a) sensitivities to EOF1 and EOF2 conditions vary across quantiles resulting in asymmetric shifts with implications for uncertainty and changes in exceedance probabilities, and (b) when EOF1 and EOF2 conditions depart significantly from median states, stationary distributional approaches systematically over and underestimate risk.

1. Given that the leading patterns of SST variability are strongly correlated with global precipitation patterns, apportioning variability from trend to SST-based covariates and stratifying variation across quantiles affords a clearer understanding of the variability in annual precipitation. Results show widespread sensitivities to EOF1, particularly in South America, Africa, the USA, and Southeast Asia. Fewer basins are sensitive to EOF2, with responses in parts of Africa, Southeast Asia, and high northern latitudes. Typologies highlight a range of single-quantile sensitivities to EOF1 and EOF2. For example, EOF1 shows increases in $\tau = 0.2$ in parts of North America with EOF2 showing decreases in $\tau = 0.2$ only. In parts of Africa, Australia, and South America, EOF1 shows decreases in both tails, while EOF2 shows the opposite response in the lower tail only. Asymmetric or single-tail responses indicate both changes in variability and risk.
2. The precipitation conditional PDF is jointly influenced by EOF1 and EOF2. Basins with significant sensitivities in either or both tails—representing large departures from median annual totals—to EOF1 and EOF2 experience a range of changes dependent on phase and magnitude. If EOF1 and EOF2 quantile-specific coefficients are of the same sign, EOF1 and EOF2 produce an additive response when in the same phase, and may minimize response when in different phases. For parts of Africa, positive EOF1 and negative EOF2 events amplify the risk of dry conditions compared to positive EOF1 and EOF2 events. QR offers an approach for assessing the SST-influenced changes across a range of quantiles, which can be applied at various spatial and temporal scales.
3. Precipitation is a primary component of water resources assessment—wet and dry periods, of short to long durations and intensity. Mischaracterization of tail-specific changes and variability has the potential of compounding error and can lead to shortcomings in assessment of risk and uncertainty. For example, Dai (2012) assessed global-warming induced drought and found widespread increase in drought risk, with many regions influenced by ENSO-induced precipitation changes. However, the results presented here show that responses in the tails to SST variability do not necessarily correspond to the mean, indicating that drought risk can be further amplified or reduced due to changes in annual total precipitation. Likewise, there are similar implications for water supply (García-García and Ummenhofer 2015; Richey et al. 2015).
4. QR is a robust method of estimating the annual precipitation distribution. QR (a) allows quantiles to move semi-independently of each other, (b) is robust to outliers,

and (c) offers a more explicit characterization of variability and implied risk. LR methods assess mean shifts but mischaracterize changes in the upper and lower quantiles. The QR model highlights sensitivities of distinct parts of the annual precipitation distribution to SST with implications for changes in risk for precipitation excesses and deficits.

In closing, we note that the analysis presented imposes a restriction of a linear model. A linear model assumes that precipitation has equal and opposite responses to positive and negative EOF1 and EOF2 phases; some deviations have been noted in a recent study (Cai et al. 2011). Furthermore, while the empirically derived patterns are uncorrelated there have been studies that show AMO modulates the amplitude of ENSO events in some regions (Power et al. 1999; Kayano and Capistrano 2014). The QR methodology and analyses presented here can be conducted for any functional form that is suited to data for a given scale and sectoral context. Assessment of precipitation at other spatial and temporal scales in the future is valuable to assessing regional or local sensitivities to climate variables for consideration in other analyses and decision-making.

Acknowledgements Climate data used in this study was downloaded from NOAA/OAR/ESRL PSD, Boulder, Colorado, USA, from their Web site at http://www.esrl.noaa.gov/psd/.

References

Bondell HD, Reich BJ, Wang H (2010) Noncrossing quantile regression curve estimation. Biometrika 97(4):825–838. https://doi.org/10.1093/biomet/asq048

Bradley RS, Diaz HF, Eischeid JK, Jones PD, Kelly PM, Goodess CM (1987) Precipitation fluctuations over Northern Hemisphere land areas since the mid-19th century. Science 237(4811):171–175. https://doi.org/10.1126/science.237.4811.171

Brauman KA, Daily GC, Duarte TK, Mooney HA (2007) The nature and value of ecosystem services: an overview highlighting hydrologic services 32(1):67–98. https://doi.org/10.1146/annurev.energy.32.031306.102758

Cai W, Van Rensch P, Cowan T, Hendon HH (2011) Teleconnection pathways of ENSO and the IOD and the mechanisms for impacts on Australian rainfall. J Climate 24(15):3910–3923. https://doi.org/10.1175/2011JCLI4129.1

Chang H, Bonnette MR (2016) Climate change and water-related ecosystem services: impacts of drought in California, USA. Ecosystem Health Sustainability 2(12):e01,254–n/a. https://doi.org/10.1002/ehs2.1254

Dai A (2012) Increasing drought under global warming in observations and models. Nat Clim Change 3(1):52–58. https://doi.org/10.1038/nclimate1633

Dai A, Wigley TML (2000) Global patterns of ENSO–induced precipitation. Geophys Res Lett 27(9):1283–1286. https://doi.org/10.1029/1999GL011140

Deser C, Alexander MA, Xie S, Phillips AS (2010) Sea surface temperature variability: patterns and mechanisms. Annu Rev Mar Sci 2(1):115–143. https://doi.org/101146/annurev-marine-120408-151453

Diaz H, Markgraf V (2000) Multiscale variability and global and regional impacts. Cambridge University Press, Cambridge

Diaz HF, Bradley RS, Eischeid JK (1989) Precipitation fluctuations over global land areas since the late 1800's. J Geophys Res 94(D1):1195–1210. https://doi.org/10.1029/JD094iD01p01195

Enfield DB, MestaNuñez AM, Trimble PJ (2001) The Atlantic multidecadal oscillation and its relation to rainfall and river flows in the continental US. Geophys Res Lett 28(10):2077–2080. https://doi.org/10.1029/2000GL012745

García-García D, Ummenhofer CC (2015) Multidecadal variability of the continental precipitation annual amplitude driven by AMO and ENSO. Geophys Res Lett 42(2):526–535. https://doi.org/10.1002/2014GL062451

Gershunov A, Barnett TP (1998) ENSO influence on intraseasonal extreme rainfall and temperature frequencies in the contiguous United States: observations and model results. J Climate 11(7):1575–1586. https://doi.org/10.1175/1520-0442(1998)011<1575:EIOIER>20CO;2

Global Runoff Data Centre (GRDC) (2007) Major River Basins of the World/ Global Runoff Data Centre. Federal Institute of Hydrology (BfG)

Groisman PY, Easterling DR (1994) Variability and trends of total precipitation and snowfall over the United States and Canada. J Climate 7(1):184–205. https://doi.org/10.1175/1520-0442(1994)007<0184:VATOTP>20CO;2

Harris I, Jones PD, Osborn TJ, Lister DH (2014) Updated high-resolution grids of monthly climatic observations—the CRU TS3.10 Dataset. Int J Climatol 34(3):623–642. https://doi.org/10.1002/joc.3711

Jolliffe I (2002) Principal component analysis. Springer, Berlin

Jones P (1988) Large-scale precipitation fluctuations: a comparison of grid-based and areal precipitation estimates. In: Gregory S (ed) Recent climatic change, 2nd edn. Belhaven Press, pp 30-40

Karl TR, Knight RW, Plummer N (1995) Trend in high-frequency climate variability in the twentieth century. Nature 377:217–220. https://doi.org/10.1002/qj49712152509

Kayano MT, Capistrano VB (2014) How the Atlantic multidecadal oscillation (AMO) modifies the ENSO influence on the South American rainfall. Int J Climatol 34(1):162–178. https://doi.org/10.1002/joc3674

Kenyon J, Hegerl GC (2010) Influence of modes of climate variability on global precipitation extremes. J Climate 23(23):6248–6262. https://doi.org/10.1175/2010JCLI3617.1

Kim JS, Jain S (2011) Precipitation trends over the Korean peninsula: typhoon-induced changes and a typology for characterizing climate-related risk. Environ Res Lett 6:034,033. https://doi.org/10.1088/1748-9326/6/3/034033

Knight JR, Folland CK, Scaife AA (2006) Climate impacts of the Atlantic multidecadal oscillation. Geophys Res Lett 33:17. https://doi.org/10.1029/2006GL026242

Koenker R (2005) Quantile regression. Cambridge University Press, Cambridge

Koenker R (2017) Quantile regression: 40 years on 9(1). https://doi.org/10.1146/annurev-economics-063016-103651

Koenker R, Bassett G (1978) Regression quantiles. Econometrica 46(1):33–50

Lee K, Baek HJ, Cho C (2013) Analysis of changes in extreme temperature using quantile regression. Asia-Pacific J Atmos Sci 49(3):313–323. https://doi.org/10.1007/s13143-013-0030-1

Messié M, Chavez F (2011) Global modes of sea surface temperature variability in relation to regional climate indices. J Climate 24(16):4314–4331. https://doi.org/10.1175/2011JCLI39411

Nigam S, Guan B, Ruiz-Barradas A (2011) Key role of the Atlantic multidecadal oscillation in 20th century drought and wet periods over the Great Plains. Geophys Res Lett 38:16. https://doi.org/10.1029/2011GL048650

Power S, Casey T, Folland C, Colman A, Mehta V (1999) Inter-decadal modulation of the impact of ENSO on Australia. Clim Dynam 15(5):319–324. https://doi.org/10.1007/s003820050284

Richey AS, Thomas BF, Lo M, Reager JT, Famiglietti JS, Voss K, Rodell M (2015) Quantifying renewable groundwater stress with GRACE. Water Resour Res 51(7):5217–5238. https://doi.org/10.1002/2015WR017349

Scaife AA, Folland CK, Alexander LV, Moberg A, Knight JR (2008) European climate extremes and the North Atlantic oscillation. J Climate 21(1):72–83. https://doi.org/10.1175/2007JCLI1631.1

Smith TM, Reynolds RW, Peterson TC, Lawrimore J (2008) Improvements NOAAs historical merged land-ocean temp analysis (1880–2006). J Climate 21:10. https://doi.org/10.1175/2007JCLI2100.1

Sun X, Renard B, Thyer M, Westra S, Lang M (2015) A global analysis of the asymmetric effect of ENSO on extreme precipitation. J Hydrol 530:51–65. https://doi.org/10.1016/j.jhydrol.2015.09.016

Sutton R, Hodson DLR (2005) Atlantic ocean forcing of North American and European summer climate. Science 309(5731):115–118. https://doi.org/10.1126/science.1112666

Trenberth K, Jones P, Ambenje P, Bojariu R, Easterling D, Tank AK, Parker D, Rahimzadeh F, Renwick J, Rusticucci M, Soden B, Zhai P (2007) Observations: surface and atmospheric climate change. In: Climate change 2007: The physical science basis. Cambridge University Press

Whan K, Zwiers F (2017) The impact of ENSO and the NAO on extreme winter precipitation in North America in observations and regional climate models. Clim Dynam 48(5):1401–1411. https://doi.org/10.1007/s00382-016-3148-x